

The Effect of HVOF Bond Coating with APS Flash Coating on TBC Performance

M. J. Lance, B. P. Thiesing, J. A. Haynes, C. M. Parish and B. A. Pint

Materials Science and Technology Division

Oak Ridge National Laboratory, 1 Bethel Valley Rd., Oak Ridge, TN 37831, USA

Abstract

To study the benefit of ~50 µm thick air plasma sprayed (APS) ‘flash’ bond coatings, NiCoCrAlYHfSi high-velocity oxygen fuel (HVOF) bond coatings were deposited on alloy 247 disk substrates with APS yttria-stabilized zirconia top coatings. Using 1-h cycles at 1100 °C in air with 10% H₂O and HVOF-only bond coatings as a baseline, APS flash coatings extended the average coating lifetime by >10% using NiCoCrAlYHfSi and >70% using NiCoCrAlY powder. Coatings were characterized after 0, 100 and 300 cycles and after failure. Residual stress in the thermally-grown alumina scale was mapped every 100 cycles using photo-stimulated luminescence piezospectroscopy. The flash coating created an interlocked metal-alumina layer that appeared to inhibit critical crack formation and the underlying HVOF layer prevented further internal oxidation and appeared to supply the APS flash coating with Al. The addition of Hf and Y to the flash coating increased internal oxidation and accelerated Al consumption, thereby reducing the benefit of the flash coating.

Keywords: photo-stimulated luminescence piezospectroscopy (PLPS); furnace cycle testing (FCT); APS flash coating; alumina scale; TBC; HVOF bond coating

Corresponding Author: Michael J. Lance, lancem@ornl.gov, 865-241-4536, ORCID: 0000-0001-5167-5452

Notice: This manuscript has been authored by UT-Battelle, LLC under Contract No. DE-AC05-00OR22725 with the U.S. Department of Energy. The United States Government retains and the publisher, by accepting the article for publication, acknowledges that the United States Government retains a non-exclusive, paid-up, irrevocable, world-wide license to publish or reproduce the published form of this manuscript, or allow others to do so, for United States Government purposes. The Department of Energy will provide public access to these results of federally sponsored research in accordance with the DOE Public Access Plan (<http://energy.gov/downloads/doe-public-access-plan>).

1. Introduction

The previous work showed that an MCrAlY air plasma sprayed (APS) ‘flash’ coating above a dense high velocity oxy-fuel (HVOF) coating could significantly increase thermal barrier coating (TBC) lifetime in furnace cycle testing (FCT) [1,2]. The longer lifetime was attributed to enhanced micro-roughness compared to conventional HVOF coatings. In a second study [3], the enhanced lifetime of these two-layer bond coatings was attributed to the lower coefficient of thermal expansion (CTE) of the flash coating due to internal oxidation and porosity which more closely matched the yttria-stabilized zirconia (YSZ) top coat. Recently [2], a large increase in average TBC lifetime was found when an APS flash coating was applied to superalloy 247 rod specimens that had surprisingly short lifetimes with an HVOF-only MCrAlYHfSi [4] bond coating using 100-h cycles in air with 10% H_2O (wet air) at 1100°C, Fig. 1. Wet air was used to better simulate the exhaust environment of a turbine engine [5,6].

In order to compare the effect of a flash coating to prior FCT results using 1-h cycles in wet air at 1100°C [7,8], this study returned to flat disk specimens of alloy 247 to quantify the benefit of the APS flash coating observed on the rods and to monitor the evolution of the residual stress in the thermally grown alumina scale using photo-stimulated luminescence piezospectroscopy (PLPS) [5,6,9-12]. The performance of APS flash coatings with MCrAlY and MCrAlYHfSi powders were compared to HVOF-only bond coatings [7,13], and all three types of bond coatings were coated with a standard APS YSZ top coating made in the same batch.

2. Material and methods

Alloy 247 superalloy disks (1.59 cm diameter and 2 mm thick with a composition shown in Table 1) were coated on one side with an HVOF NiCoCrAlYHfSi bond coating using the powder composition designated YHfSi in Table 1. For the outer APS flash coating, two different powders were used with compositions shown in Table 1. One flash coating powder (Y-only) contained only 0.42 wt.% Y, and the second flash coating powder (YHfSi) was the same powder also used for the HVOF inner bond coating layer on all specimens. One set of samples were not subsequently coated with a flash coating and so only had an HVOF coating. The starting powder size was $37.5 \pm 6.6 \mu\text{m}$ and $32.4 \pm 9.1 \mu\text{m}$ for the Y-only and YHfSi bond coating powders, respectively. All the bond and flash coatings were annealed at 1080 °C for 4 h in a 10^{-4} Pa vacuum prior to the deposition of a $\sim 200 \mu\text{m}$ thick APS YSZ top coating.

Five specimens of each coating type were thermally cycled at 1100 °C in air with 10 vol.% H₂O. The specimens were held on alumina rods using a Pt-Rh wire in an automated vertical furnace rig and each cycle consisted of 1 h at temperature followed by cooling for 10 min in ambient air to <30 °C. The specimens were removed from the rig for inspection and weighing every 20 cycles. The failure criterion was >20% coating loss but failure typically was 100% of the YSZ coating spalling in one piece. A portion of one disk of each type of flash-coated specimen was cut off for characterization using a diamond saw. The same specimen was then cycled to 100 cycles and then 300 cycles and a portion of the disk was cut off at each stage to observe the evolution of the reaction products beneath the YSZ.

Residual hydrostatic stress was nondestructively measured in the thermally-grown α -Al₂O₃ scale through the YSZ top coating after cycling using PLPS as described elsewhere [5-7,9,10,12]. A Raman microprobe (Dilor model XY800, Horiba Scientific, Edison, NJ) with an Ar⁺ laser operating at 5145 Å was used to measure the same 500 X 670 μm region with a step size of 10 μm after every 100 cycles. This allowed the local evolution of stress to be monitored during FCT for one specimen of each type of bond coating. For characterization of the reaction products, specimens were mounted in epoxy, polished and imaged using light microscopy and scanning electron microscopy (SEM). Compositional maps were acquired using energy dispersive spectroscopy (EDS).

Fractal analysis was performed on a cross-section image of each of the three bond coatings using the equation:

$$L_R = \sum_i^N \frac{1}{\cos\theta_i} \frac{p_i}{L} \quad (1)$$

where L_R is the relative length, L is the total projected length for all N virtual steps, p_i is the projected length for virtual step and θ_i is angle between the normal to the nominal surface. This is the same methodology as used by Nowak et al. [1]. For each sample, the bond coating/YSZ interface for four separate images was isolated using ImageJ and then stitched together using Inkscape. The stitched image was then analyzed by the compass-method using a MATLAB™ script which evaluated the relative length for 300 progressively smaller rulers. This yielded the relative length (L_R) as a function of scale length (r). The smooth-rough crossover was determined manually and then the fractal dimension (D_f) was extracted from the slope. The roughness of the bond coating/YSZ interface was determined by image analysis of cross-sections.

EDS spectrum images from cross-sections were analyzed using optimally-scaled principal component analysis [14], which was used to de-noise the datasets by rank-reduction to create a low-noise basis for subsequent

analysis. The subsequent analysis used was the modification of independent component analysis (ICA) described by Windig and Keenan [15], which provides better analysis of EDS data than traditional ICA methods; specifically, the first method ("appended") of the two described by Windig and Keenan was used. The ICA results are in the form of spectral endmembers representing independent elemental groupings in space, and the abundance maps are the pixel weightings of the abundances. The spectral endmembers and abundance maps produced were then exported to HDF5 and image formats. These calculations were performed using MATLAB R2018 via in-house scripts.

3. Results and discussion

Fig. 2 shows the as received cross-sections of the APS flash coatings and a representative HVOF specimen for comparison. The NiCoCrAlYHfSi HVOF-only coating appears dense across the entire bond coating as does the inner HVOF bond coating of the two bi-layer coatings. The outer APS coating of both bi-layer bond coatings (Figs. 2a & 2b) contains internal oxidation that is oriented parallel to the coating interface and is typical of the APS process [16]. The YHfSi APS outer layer appears to contain more internal oxidation than the Y-only APS outer coating. As similar powder sizes were used for each APS coating, this cannot be attributed to splat size but is more likely a result of in-flight oxidation of the higher Y and Hf levels in the YHfSi coating, Table 1. Fig. 3 shows the starting thicknesses of the three bond coatings shown in Fig. 2. The bond coating thicknesses were very similar for the two bi-layer (flash coated) samples. Due to difficulties in achieving the correct bond coating thickness, the HVOF-only bond coating was $\sim 40 \mu\text{m}$ thicker than the total thickness of the two bi-layer coatings.

Fig. 4 shows the roughness (R_a) and fractal dimension [1] at the YSZ/bond coating interface of all three as-received coatings. The roughness was higher on the two APS bi-layer coatings compared to the HVOF-only coating. However, the roughness values for all three coatings were significantly less than have been reported elsewhere [1,3]. The fractal dimension (D_f) is a measurement of the micro-roughness of the interface. Both flash coated samples had a D_f around 1.12 which was only slightly above that of the HVOF-only coating and was much lower than the D_f measured by Nowak, et al., on their flash coated sample which was 1.31 [1]. The small change in D_f between the three samples in this work suggests that the micro-roughness did not vary enough to accurately test the effect of this parameter on coating lifetime.

Fig. 5 shows the average lifetime for five specimens of each type of coating in 1-h cycles at 1100 °C in 10% H₂O and air. For comparison, the average lifetimes for two previous batches (three specimens per batch) of

similar HVOF-only bond coatings on 247 substrates are shown [9,10]. The differences among the three HVOF-only batches illustrate the variability from the multi-step coating fabrication process and confirms the need to create a baseline for each study. Unlike prior studies where lifetimes were not always statistically-significant [2,7], the YHfSi flash coating showed an increase in average lifetime of 12% while the Y-only flash coating improved the average lifetime by 71%. The longer lifetime for the Y-only flash coating was opposite to results for HVOF-only coatings where YHfSi powder outperformed an MCrAlY HVOF-only bond coating by 20-40% [17].

The mean compressive residual stress in the thermally-grown Al_2O_3 scale is shown in Fig. 6. For all three coatings, the stress gradually decreased with thermal cycling due to damage accumulation in the scale. The rate of stress decline was fastest for the HVOF-only bond coating which reached a lower mean compressive stress prior to failing than the two bi-layer coatings. Two-dimensional stress maps measured from the same area following subsequent thermal cycling on all three coatings are shown in Fig. 7. The blue regions correspond to areas of near-zero stress where the residual thermal mismatch stress between the scale and the bond coating had been relieved by cracking, especially near asperities in the bond coating as observed previously [6,7,9,10]. The stress in the HVOF-only coating was more uniform than the two APS flash coated samples, which reflects the smoother interface of the HVOF sample, Fig. 4. This lower roughness interface may also enable earlier failure of the HVOF-only bond coating by allowing a crack to traverse the interface without being deflected by an asperity in the bond coating. All three coatings gradually decreased in compressive stress within the flatter regions away from the bond coating asperities going from ~ 1.2 GPa (pink color) to ~ 0.5 GPa (green color) prior to failure.

Back-scattered electron SEM images of representative failed cross-sections of each coating type are shown in Fig. 8. The failed HVOF-only interface (Fig. 8a) had a uniform alumina scale with indications of repeated cracking [18] and appears smoother than the two APS flash coatings, which is consistent with the stress maps in Figure 7. In contrast, the two flash-coated samples (Fig. 8b & c) formed a much larger volume of oxide and the outer layer has become a coarse mixture of oxide and metal. Normally, a large amount of oxide formation and associated Al consumption does not bode well for coating performance. Yet the oxides appear to be mainly alumina and did not appear to penetrate the inner HVOF layer. Instead, the mixed metal-oxide layer may have been more compliant and prevented a crack from growing along the interface. Also, the volume expansion associated with alumina formation may have provided a compressive stress that could inhibit crack growth. This composite layer also may have reduced the CTE mismatch between the substrate and the scale. The strain energy associated with this

mismatch is the driving force for scale spallation and the critical scale thickness for spallation is proportional to the square of the CTE mismatch [19]. EDS analysis indicated that the HVOF layer beneath the YHfSi flash coating had only $3.5 \pm 0.2\%$ Al (based on spectra collected from the HVOF layer) remaining at failure after 760 cycles. In contrast, the Y-only flash coating had $4.3 \pm 0.1\%$ Al remaining after 1080 cycles, suggesting a significantly slower consumption rate. For comparison, the thicker HVOF only coating had $5.3 \pm 0.4\%$ Al after failure at 620 cycles.

The difference in average lifetime between the two flash coatings was significantly larger than expected and therefore comparing the failed microstructures is less relevant since the failure times were so different. To better understand the performance difference between the Y-only and YHfSi flash coatings, pieces were cut off one coupon of each type after 100 and 300 cycles for microstructure comparisons. Back-scattered electron SEM images and Al EDS concentration maps for both bi-layer bond coatings after 300 cycles are shown in Fig. 9. The most striking difference between the two bi-layer bond coatings is that a layer of β -NiAl (i.e. Al-rich) precipitates remained in the HVOF layer beneath the Y-only flash coating, indicated by the red arrow in Fig. 9b. This region is absent in the YHfSi bond coating (Fig. 9d) suggesting that more Al depletion had occurred from this coating after 300 cycles due to more oxide formation in the outer layer of the bond coating. Since the Al reservoir was similar in these two coatings of similar thickness, the coating with a slower Al consumption rate would be expected to have a longer lifetime. Once the coating is significantly depleted in Al, it is well-known that the formation of Cr- or Ni-rich oxides will hasten failure [20,21]. To determine what oxides formed at failure of the flash coatings, Figure 10 shows independent component analyses of EDS maps following failure. Both failed oxide scales contain Cr-rich oxides near the YSZ top coating, Figs. 10c and 10f. [22]. These oxides may have formed through the diffusion cell effect described by Evans and Taylor [21].

The higher Y and Hf (i.e. reactive element (RE)) content in the YHfSi flash coating (Table 1) appeared to lead to more internal oxidation in the as-sprayed coating (cf. Figs. 2b & c) [23]. During cycling, this coating also appeared to form more oxide in the outer layer resulting in more rapid Al depletion and earlier failure in the cyclic test. Fig. 11 focuses on the APS flash coating layer from the Y-only and YHfSi coatings after 100 and 300 cycles at 1100 °C. Both flash coatings contain voids in the internally oxidized areas which will help to reduce the stiffness of the flash coating region. A more compliant interface could reduce the thermal mechanical stresses which will enhance coating lifetime. Nevertheless, the benefits of having an APS flash coating layer were partially offset for the

YHfSi flash coating by too much internal oxidation. Optimization of the RE addition for a flash coating may be different than optimal levels for other types of bond coatings [24].

Additional three-dimensional characterization of the outer bond coating layer is in progress. It appears that this layer assists in preventing cracks from propagating along the interface as suggested by Nowak, et al. [1]. Traditionally, efforts to create graded metal-oxide bond coatings [25] have encountered issues with Al depletion from the metallic phase leading to early failure due to Ni-rich oxide formation. With the bi-layer coating structure, the inner HVOF layer appears to confine the mixed metal-oxide structure to the outer layer and likely supplies Al to the metal in this layer. Once pathways for the Al to diffuse to the metal tendrils in the intermixed layer from the dense HVOF layer are cut off due to oxidation, the outer layer will become Al depleted and begin to form other oxides. Similar structures were observed by Zou et al. [3] but not by Nowak et al. [1]. Based on how the outer layer oxidation develops, it is not clear how important starting roughness is to the improvement in FCT lifetime. Further work is needed comparing flash coatings with different starting roughness. Comparing coatings with different inner and outer layer thicknesses also might determine the importance of the inner layer acting as an Al reservoir.

4. Conclusion

The effect of two different flash coatings on average TBC lifetime was studied in furnace cycle testing using 1-h cycles in wet air at 1100 °C. Two types of flash coatings applied over an NiCoCrAlYHfSi HVOF layer increased the lifetime compared to an HVOF-only bond coating that was greater in thickness. However, the NiCoCrAlYHfSi flash coating only increased the average furnace cycle lifetime by ~10% because of excessive oxidation and Al consumption associated with the higher Y and Hf levels in this outer layer. The NiCoCrAlY flash coating increased the average lifetime by ~70%. In both cases, the outer APS layer converted into a convoluted mixture of interlocking metal and oxide that retained a higher residual stress in the alumina than a conventional HVOF-only coating. The inner HVOF layer prevented further ingress of the oxide and supplied Al to the outer layer. The development of this mixed outer layer does not necessarily support the hypothesis that starting coating roughness predicts lifetime and this correlation should be further investigated using flash coatings of different starting roughness on both disk and rod specimens.

Acknowledgements

The authors would like to thank Prof. S. Sampath and E. Gildersleeve at Stony Brook University's Center for Thermal Spray Research for the coating fabrication. At ORNL, G. Garner, T. Lowe, T. Geer, and T. Jordan assisted with the experimental work and S. N. Dryepont, A. A. Wereszczak and E. Lara-Curzio provided helpful comments on the manuscript. This research was sponsored by the U.S. Department of Energy, Office of Fossil Energy, Turbine Program (R. Dennis program manager and P. Burke project manager).

References

- 1 Nowak W, Naumenko D, Mor Get al. Effect of processing parameters on MCrAlY bondcoat roughness and lifetime of APS-TBC systems *Surf. Coat. Technol.* 2014;260:82-89.
- 2 Pint BA, Lance MJ, Haynes JA. The effect of coating composition and geometry on TBC lifetime *J. Eng. Gas Turb. & Power.* 2019;141:031004.
- 3 Zou Z, Jia L, Yang Let al. . Role of internal oxidation on the failure of air plasma sprayed thermal barrier coatings with a double-layered bond coat *Surf. Coat. Technol.* 2017;319:370-377.
- 4 Demasi-Marcin JT, Gupta DK. Protective coatings in the gas turbine engine *Surf. Coat. Technol.* 1994;68:1-9.
- 5 Lance MJ, Unocic KA, Haynes JA, Pint BA. Effect of water vapor on thermally-grown alumina scales on Pt-modified and simple aluminide bond coatings *Surf. Coat. Technol.* 2013;237:2-7.
- 6 Lance MJ, Unocic KA, Haynes JA, Pint BA. The effect of cycle frequency, H₂O and CO₂ on TBC lifetime with NiCoCrAlYHfSi bond coatings *Surf. Coat. Technol.* 2014;260:107-112.
- 7 Lance MJ, Haynes JA, Pint BA. Performance of vacuum plasma spray and HVOF bond coatings at 900° and 1100 °C *Surf. Coat. Technol.* 2018;337:136-140.
- 8 Pint BA, Haynes JA, Lance MJ, et al. Factors affecting TBC furnace cycle lifetime: temperature, environment, structure and composition. *Superalloys 2016*; John Wiley & Sons, Inc.;2016:727-734.
- 9 Lance MJ, Haynes JA, Pint BA. The effects of temperature and substrate curvature on TBC lifetime and residual stress in alumina scales beneath APS YSZ *Surf. Coat. Technol.* 2016;308:19-23.
- 10 Lance MJ, Unocic KA, Haynes JA, Pint BA. APS TBC performance on directionally-solidified superalloy substrates with HVOF NiCoCrAlYHfSi bond coatings *Surf. Coat. Technol.* 2015;284:9-13.
- 11 Lipkin DM, Clarke DR. Measurement of the Stress in Oxide Scales Formed by Oxidation of Alumina-Forming Alloys *Oxid. Met.* 1996;45:267-280.
- 12 Nychka JA, Clarke DR. Damage quantification in TBCs by photo-stimulated luminescence spectroscopy *Surf. Coat. Technol.* 2001;146:110-116.
- 13 Pint BA, Unocic KA, Haynes JA. The Effect of Environment on TBC Lifetime *J. Eng. Gas Turb. & Power.* 2016;138:082102.

- 14 Keenan MR, Kotula PG. Optimal scaling of TOF-SIMS spectrum-images prior to multivariate statistical analysis *Applied Surface Science*. 2004;231:240-244; Keenan MR, Kotula PG. Accounting for Poisson noise in the multivariate analysis of ToF-SIMS spectrum images *Surface and Interface Analysis*. 2004;36:203-212; Keenan MR. Multivariate Analysis of Spectral Images Composed of Count Data. In: Grahn HF, Geladi P, *Techniques and Applications of Hyperspectral Image Analysis*, John Wiley & Sons, Ltd. ;2007:89-126.
- 15 Windig W, Keenan MR. Homeopathic ICA: A simple approach to expand the use of independent component analysis (ICA) *Chemometrics and Intelligent Laboratory Systems*. 2015;142:54-63.
- 16 Haynes JA, Ferber MK, Porter WD. Thermal cycling behavior of plasma-sprayed thermal barrier coatings with various MCrAlX bond coats *J. Therm. Spray Technol*. 2000;9:38-48.
- 17 Haynes JA, Unocic KA, Pint BA. Effect of water vapor on the 1100°C oxidation behavior of plasma-sprayed TBCs with HVOF NiCoCrAlX bond coatings *Surf. Coat. Technol*. 2013;215:39-45.
- 18 Naumenko D, Shemet V, Singheiser L, Quadackers WJ. Failure mechanisms of thermal barrier coatings on MCrAlY-type bondcoats associated with the formation of the thermally grown oxide *J Mater Sci*. 2009;44:1687-1703.
- 19 Evans HE. Stress effects in high temperature oxidation of metals *International Materials Reviews*. 1995;40:1-40.
- 20 Rensch D, Schorr M, Schutze M. The role that bond coat depletion of aluminum has on the lifetime of APS-TBC under oxidizing conditions *Mater. Corros*. 2008;59:547-555; Sloof WG, Nijdam TJ. On the high-temperature oxidation of MCrAlY coatings *Inter. J. Mater. Res*. 2009;100:1318-1330.
- 21 Evans HE, Taylor MP. Diffusion cells and chemical failure of MCrAlY bond coats in thermal-barrier coating systems *Oxid. Met*. 2001;55:17-34.
- 22 Lih W, Chang E, Wu BC, Chao CH. Effects of bond coat preoxidation on the properties of ZrO₂-8wt-percent Y₂O₃/Ni-22Cr-10Al-1Y thermal-barrier coatings *Oxidation of Metals*. 1991;36:221-238; Demasi-Marcin JT, Sheffler KD, Bose S. Mechanisms of degradation and failure in a plasma-deposited thermal barrier coating *J. Eng. Gas. Turbines Power-Trans. ASME*. 1990;112:521-526.
- 23 Pint BA. Optimization of Reactive-Element Additions to Improve Oxidation Performance of Alumina-Forming Alloys *J. Amer. Cer. Soc*. 2003;86:686-695.

- 24 Naumenko D, Pint BA, Quadackers WJ. Current Thoughts on Reactive Element Effects in Alumina-Forming Systems: In Memory of John Stringer *Oxid. Met.* 2016;86:1-43.
- 25 Kim JH, Kim MC, Park CG. Evaluation of functionally graded thermal barrier coatings fabricated by detonation gun spray technique *Surf. Coat. Technol.* 2003;168:275-280; Kokini K, DeJonge J, Rangaraj S, Beardsley B. Thermal shock of functionally graded thermal barrier coatings with similar thermal resistance *Surf. Coat. Technol.* 2002;154:223-231; Demirkiran AS, Celik E, Yargan M, Avcı E. Oxidation behaviour of functionally gradient coatings including different composition of cermets *Surf. Coat. Technol.* 2001;142:551-556.

Table 1. Chemical compositions (weight % or ppmw) determined by inductively coupled plasma analysis and combustion analysis.

Material	Ni	Co	Cr	Al	Y	Hf	Si	Ti	W	Ta	Mo	C	Other (ppmw)
Y-only powder	47.1	23.0	16.6	12.8	0.42	<	0.04	<	0.02	<	<	<	8 S
YHfSi powder	48.0	21.6	16.7	12.3	0.68	0.25	0.36	<	0.01	<	<	<	2 S
Alloy 247	59.1	10.2	8.5	5.6	<	1.32	0.06	1.0	10.0	3.2	0.6	0.2	200 Re, 11 S

< indicates below the detectability limit of <0.01%.

List of figure captions

Figure 1. TBC rod lifetimes (cycles to failure) following 100-h cycles in air + 10 vol.% H₂O at 1100 °C. The error bars are one standard deviation of 3 measurements about the mean value.

Figure 2. Light optical microscope images of polished cross-sections of as received (a) YHfSi HVOF-only, (b) Y-only Bi-layer, and (c) YHfSi Bi-layer bond coatings.

Figure 3. The starting bond coating thicknesses of all three specimens. The error bars are one standard deviation of 30 measurements.

Figure 4. The starting roughness, R_a , and the fractal dimension (D_f) of the three bond coatings measured at the YSZ bond coating interface.

Figure 5. TBC lifetimes (cycles to failure) following 1-h cycles in air + 10 vol.% H₂O at 1100 °C of disk specimens. The error bars are one standard deviation of 5 measurements for the three specimens on the left and of 3 measurements of the two specimens on the right. The HVOF 2014 and 2015 samples were previously described in Refs. [9] and [10], respectively.

Figure 6. Mean compressive stress measured in the Al₂O₃ scale using PLPS versus number of 1-h cycles at 1100 °C of the three TBCs studied in this work. The measurements are the average of 3468 individual stress measurements and the error bars are one standard deviation. Measurements were collected every 100 cycles and the data points are shifted slightly for clarity. The cycles at failure are shown next to the last data point for each of the three TBCs.

Figure 7. Two-dimensional scale stress maps collected from the scale layer under the YSZ top coating from the three bond coatings (rows) after 20, 300, 600 and 1000 cycles (columns) at 1100 °C. Only the Y-only Bi-layer bond coating survived to 1000 cycles.

Figure 8. Back-scatter SEM images of polished cross-sections of (a) the YHfSi HVOF-only bond coating after failure at 620 c, (b) the Y-only Bi-layer bond coating after failure at 1080 c, and (c) the YHfSi Bi-layer bond coating after failure at 760 c. All cycling took place at 1100 °C in air + 10vol.% H₂O.

Figure 9. Back-scatter SEM images of (a) the Y-only Bi-layer bond coating and (c) the YHfSi Bi-layer bond coating after 300 cycles at 1100 °C. The corresponding aluminum weight percentage maps measured using

EDS are shown in (b) and (d), respectively. A region of β -phase in the Y-only Bi-layer is indicated by an arrow. The color bar was scaled so as to highlight the Al concentration in the bond coating.

Figure 10. Secondary electron images of (a) the failed Y-only Bi-layer coating after 1080 cycles and (d) the failed YHfSi Bi-layer bond coating after 760 cycles. Independent component analyses of the EDS maps show the location of Al_2O_3 and Cr-rich oxides phases for (b & c) the Y-only coating and (e & f) the YHfSi coating. The corresponding spectral endmembers for the maps in e & f are shown in (g) for the YHfSi flash coating. The Y-only flash coating showed nearly identical spectral endmembers and so, for clarity, is not displayed here.

Figure 11. Back-scatter scanning electron microscope images of polished cross-sections of the APS flash bond coating layer from (a) the Y-only Bi-layer coating after 100 cycles and (b) 300 cycles and (c) the YHfSi Bi-layer coating after 100 cycles and (d) 300 cycles. All cycling took place at 1100 °C in air + 10vol.% H_2O .

Fig 1

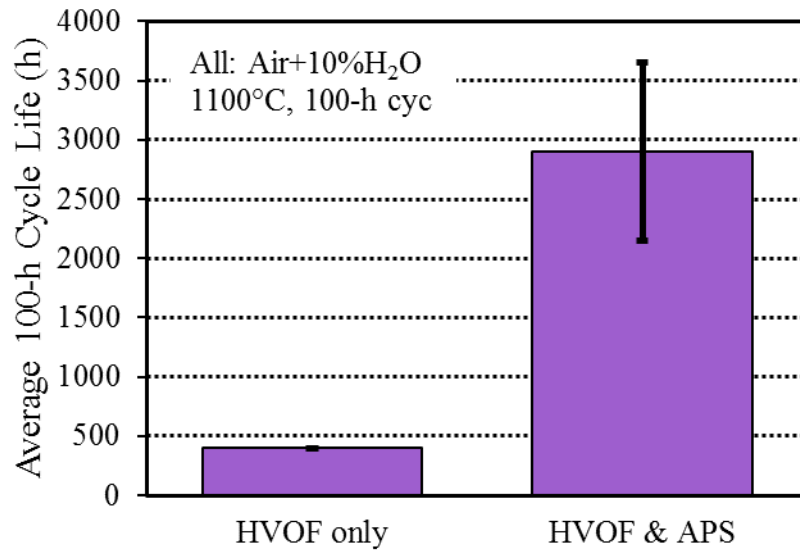


Fig 2

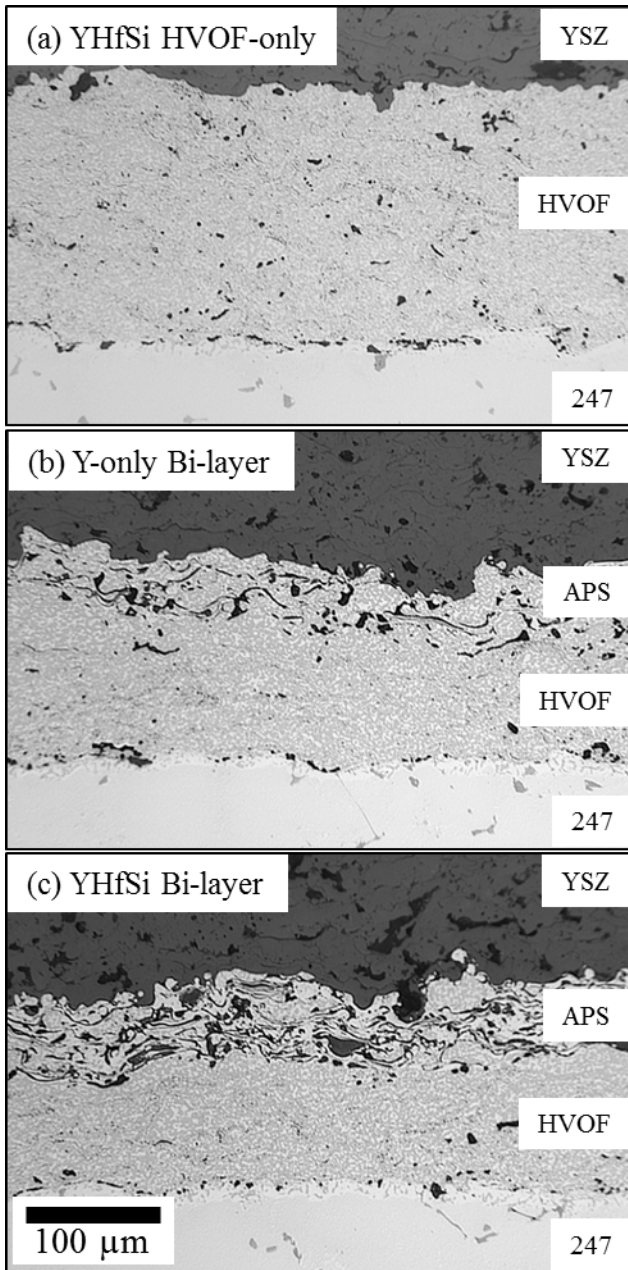


Fig 3

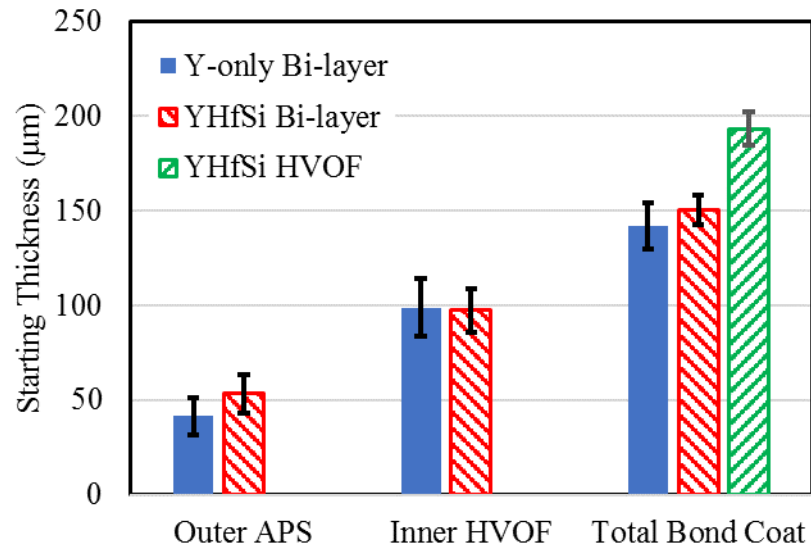


Fig 4

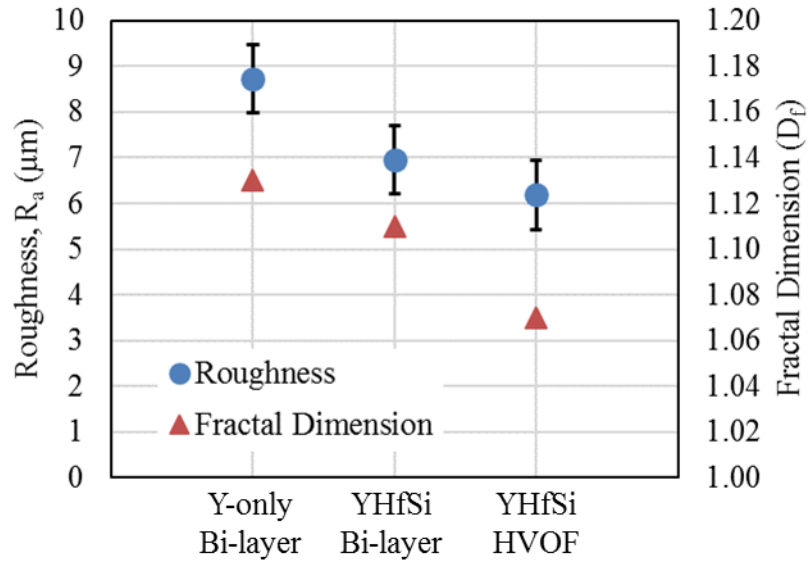


Fig 5

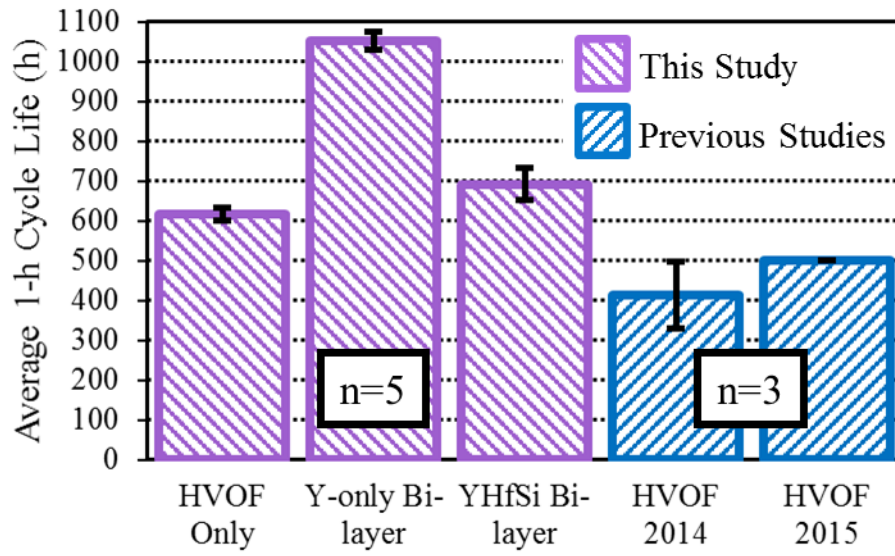


Fig 6

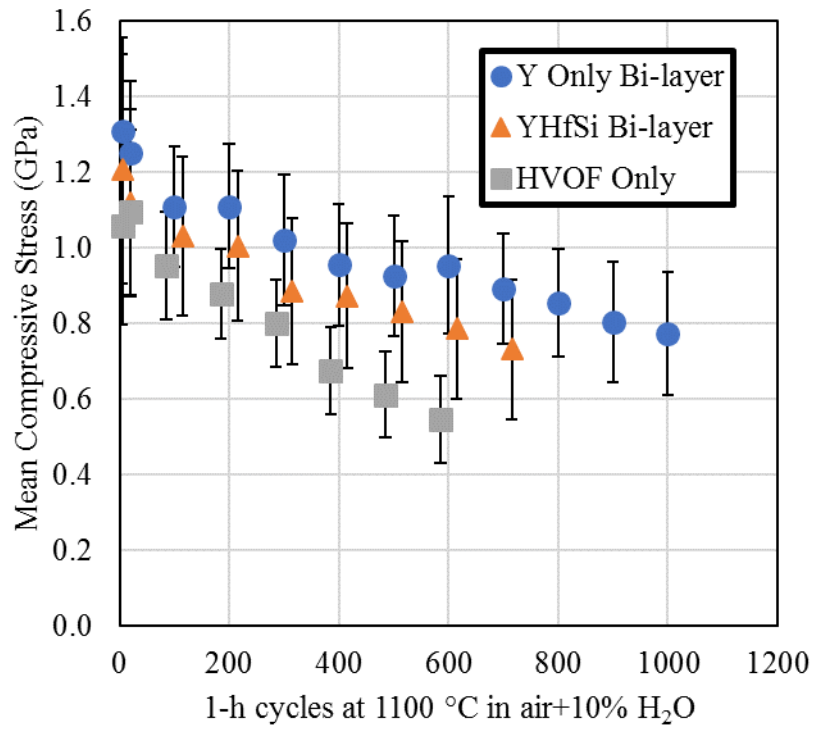


Fig 7

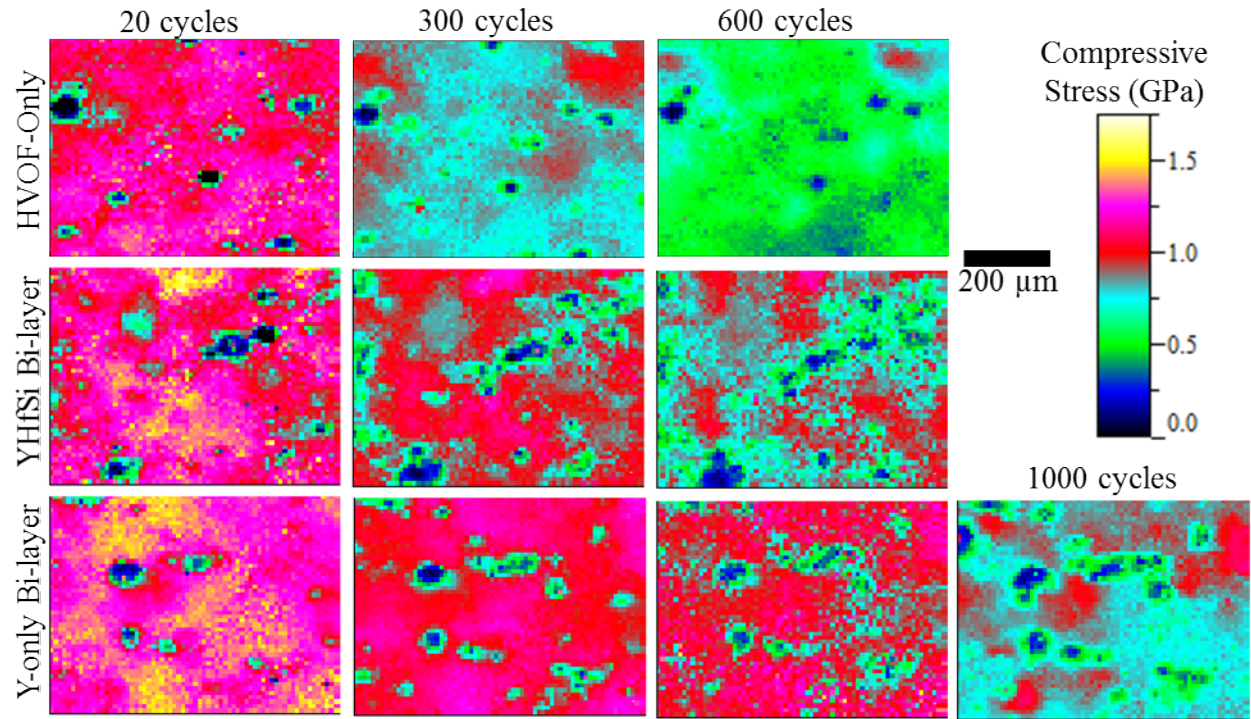


Fig 8

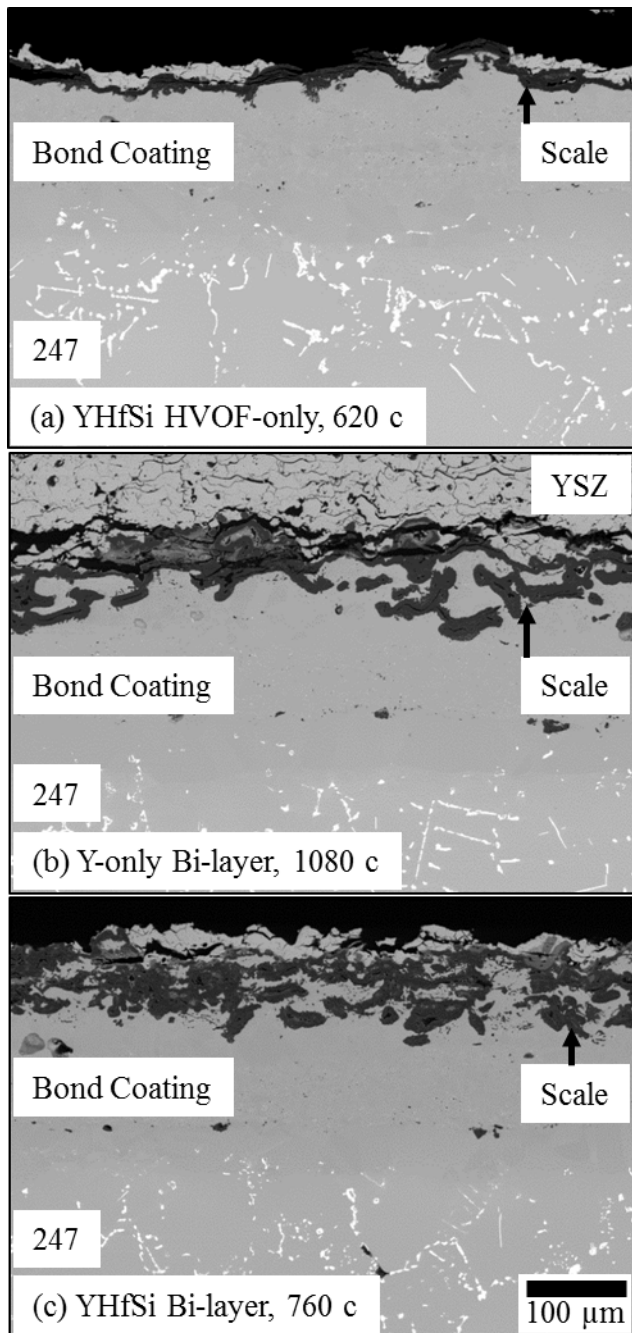


Fig 9

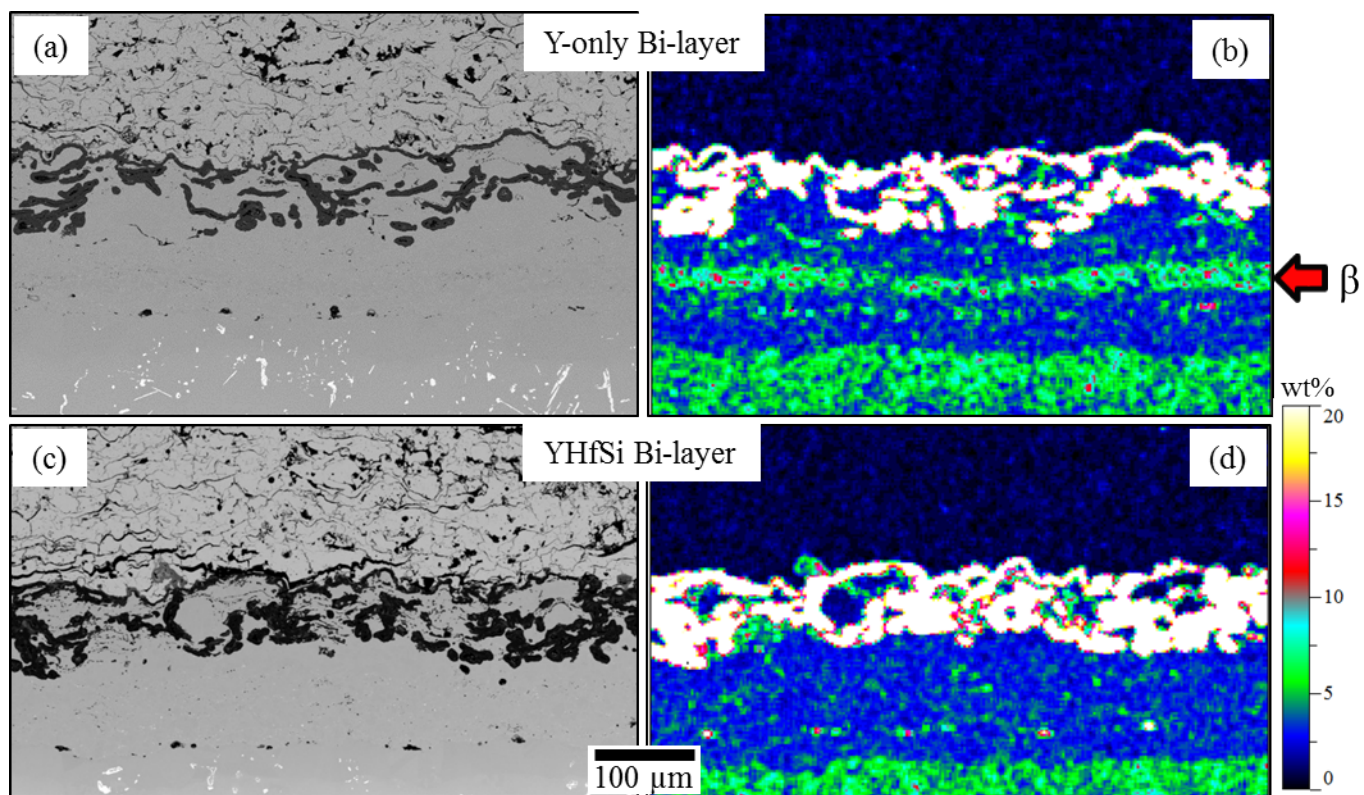


Fig 10

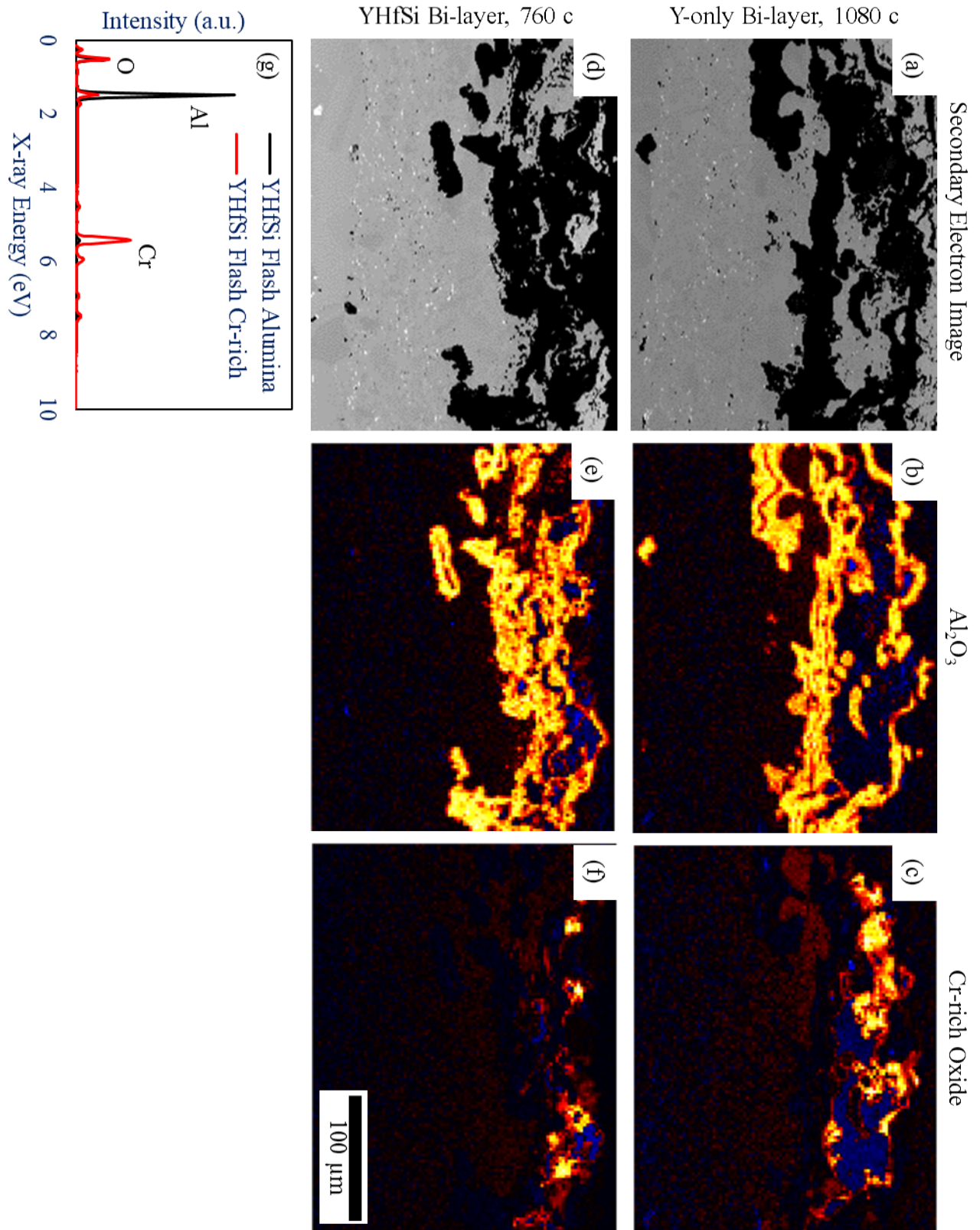


Fig 11

